



Article

Drought Effects on Photosynthesis and Implications of Photoassimilate Distribution in ^{11}C -Labeled Leaves in the African Tropical Tree Species *Maesopsis eminii* Engl.

Jackie Epila [†] , Michiel Hubeau [†]  and Kathy Steppe ^{*}

Laboratory of Plant Ecology, Department of Plants and Crops, Faculty of Bioscience Engineering, Ghent University, Coupure Links 653, 9000 Gent, Belgium; EpilaJackie@yahoo.co.uk (J.E.); Michiel.Hubeau@UGent.be (M.H.)

^{*} Correspondence: Kathy.Steppe@UGent.be; Tel.: +32-9-264-6112

[†] These authors contributed equally to this work.

Received: 13 January 2018; Accepted: 26 February 2018; Published: 28 February 2018

Abstract: Photoassimilate distribution inside leaves is less studied than photosynthesis, and yet the topic is important as it gives insights into the vital roles played by leaves in plant survival. We combined greenhouse measurements of light response curves with ^{11}C -labelling using leaves of 3-year-old potted *Maesopsis eminii* Engl. trees to improve our understanding of its leaf carbon physiology. This fast-growing pioneer tree species showed low photosynthetic rates for a common tropical pioneer during well-watered reference conditions ($5.0 \pm 0.7 \mu\text{mol m}^{-2} \text{s}^{-1}$), which further decreased in response to drought. ^{11}C -autoradiography indicated active phloem loading and/or rapid phloem transport rates. Active loading is uncommon in tree species, but might be related to deciduousness traits and continuous investment in growth, like in herbaceous active loaders. Active loading involves higher carbon allocation to growth, which might explain why low photosynthetic rates were observed in this fast-growing species. These findings suggest that examining photoassimilate distribution and transport may be critical for understanding the role tree physiology plays in terrestrial carbon cycling.

Keywords: African tropical tree; ^{11}C autoradiographs; drought; light response curve; *Maesopsis eminii* Engl.; photoassimilate distribution; leaf carbon balances; leaf photosynthesis and respiration

1. Introduction

Changes in temperature, precipitation, CO_2 , and evapotranspiration are already eminent in African tropical rainforests, affecting their ecological processes [1]. These effects have gained increasing attention [2–10] as the biome represents 15% of worldwide forests, and dominates inter-annual carbon cycling with 50% [11,12]. Concerned stakeholders are calling for investigative studies on the impact of climate change on carbon cycling processes in this terrestrial ecosystem [11–14]. Carbon-related studies carried out thus far entail measurements of photosynthesis, respiration and plant carbon budgets [11,13,15–21], and modeling that is often used to simulate and predict carbon budgets on large spatial scale [13,14]. Research seldom illustrates how photoassimilates are distributed inside the leaf, and are subsequently transported into the phloem, despite these being important plant functional characteristics [22]. Furthermore, there is a demand for more data for the African tropics [13,14] to improve CO_2 flux modeling [23,24]. Evidence is increasing that considerable uncertainties exist in assessing tropical carbon stocks [25–27], feeding the debate on how to implement tropical biomass models [28]. This points to the relevance of increasing our knowledge on the ecophysiological mechanisms underlying carbon sequestration.

Photosynthesis, respiration, carbon transport and allocation are closely linked [22,28–31], and important to understand plant carbon balances [22]. Moreover, the impact of water status on these physiological processes is manifold [22,32–36], pointing to the importance of an adequate understanding of plant drought responses for their application and up scaling into large scale models [37–39]. Besides photosynthesis, distribution of photoassimilate inside the leaf and their transport out of the leaf into the phloem are hence important aspects to consider when assessing plant carbon fluxes and growth rates [22,40].

Annually, trees in the tropics are subjected to drought resulting from a dry season. Tropical trees have different drought coping mechanisms or strategies. Some trees lose their leaves, some are semi-deciduous and others are evergreen. While an evergreen strategy may lead to more carbon gain with increasing growing season, deciduous species are expected to benefit during droughts associated with climate change [41]. To increase knowledge on species-specific carbon cycling, we have chosen *Maesopsis eminii* Engl., which is a widespread pioneer drought-deciduous tree species, mainly occurring in African tropical rainforests, and which has shown species-specific responses to drought. *M. eminii* has considerable nocturnal sap flow [42,43], which according to Caird [44] might enhance photosynthetic activity, and might be related to stem photosynthesis [45]. Furthermore, Van Camp et al. [43] found that during initial drought, root pressure mitigated drought effects on stem water storage, and Epila et al. [46] showed a substantial hydraulic capacitance in *M. eminii* that contributes to the redistribution of leaf water from more drought affected to healthier leaves in order to support survival during drought [46]. Because seedlings and saplings have an important ecological role [47,48], this study investigated leaves of 3-year-old *M. eminii* plants under well-watered and drought conditions.

To quantify *M. eminii*'s photosynthesis, respiration, photoassimilate distribution and phloem loading strategy we used a combination of techniques: (i) light response curves to assess *M. eminii*'s leaf photosynthetic performance during drought, shortly after re-watering, and after a long recovery period of 4 months (which represents well-watered reference conditions) [49–51]; (ii) ^{13}C stable isotope analysis to determine its metabolic pathway for carbon fixation [52,53]; and (iii) ^{11}C -autoradiography to map carbon distribution and phloem loading by exposing leaves to $^{11}\text{CO}_2$ [35,54–56]. Our specific working hypothesis were: (i) the pioneer *M. eminii* will have high photosynthetic rates to accommodate its fast growth, which will result in a substantially higher amount of fixed to respired carbon; and (ii) being a tree, passive loading of sugars into the phloem is expected, with ^{11}C -autoradiographs depicting a relatively uniform distribution of tracer in the mesophyll and a low accumulation of carbon tracer in the vascular bundle.

2. Materials and Methods

2.1. Site Description

The study was conducted between 5 May and 9 September 2015 in a tropical greenhouse (6.4 m wide, 9.6 m long and 4.75 m high) of Ghent University, Belgium (50°59.58' N, 3°47.04' E). Light within the greenhouse was supplied by natural solar radiation in combination with nine Philips bulbs of 200 W. A 14-h photoperiod was used, with lights turned on between 07:00 and 21:00. During the photoperiod, an average photosynthetic active radiation (PAR) of $708 \pm 27 \mu\text{mol m}^{-2} \text{s}^{-1}$ and an average daily maximum PAR of $1563 \pm 39 \mu\text{mol m}^{-2} \text{s}^{-1}$ were recorded ($N = 92$). The light intensities were within the range reported (resp. $672 \pm 55 \mu\text{mol m}^{-2} \text{s}^{-1}$ and $1727 \pm 31 \mu\text{mol m}^{-2} \text{s}^{-1}$, $N = 115$) for a study conducted on 15-months-old *M. eminii* trees in Uganda [42]. Air temperature ranged between 18 °C and 35 °C, and relative humidity of the air was set at 70%. A HortiMaX MT/MTV sensor unit (HortiMaX, Maasdijk, The Netherlands) measured the interior microclimate.

2.2. Experimental Set-Up

Fifteen 3-year-old *Maesopsis eminii* Engl. trees were used in this study, which had a height of 2.3 ± 0.4 m at the start of the experiment and a stem diameter of 21 ± 5 mm, measured at 40 cm above

the root collar. The trees were grown in 35-L bottom-perforated pots containing peat soil, and were germinated from randomly picked seeds of unselected parent plants thriving in Mabira forest, Uganda (0°23.357' N, 33°0.344' E). Trees were randomly distributed on tables raised to a height of 0.75 m and during drought periods round plastic pot saucers were used to prevent any water uptake from the tables. During periods with irrigation, trees were irrigated three times a day for four minutes using an automatic flood-table irrigation system to ensure unstressed reference conditions with ample soil water. Irrigation water consisted of a mix of rainwater and soluble fertilizer (N:P:K:Mg ratio: 19:8:16:4, boron (0.02%), copper (0.03%), iron (0.038%), manganese (0.05%), molybdenum (0.02%) and zinc (0.01%) that resulted in a solution pH of 5.7.

The experiment started with a two-week drought period, which was the consequence of an irrigation malfunctioning during this period. Photosynthesis measurements were taken at the final day of this accidental drought period, after a short time of recovering and after a 4-month recovering window, which we assumed as fully recovered, because new leaves were then mature, and the trees had grown as ample water was provided. This experiment was performed in controlled greenhouse conditions, but could be used as a proxy of tropical trees' behavior during the dry season and their recovery in the wet season.

2.3. Photosynthesis Measurements

Light response curves were measured after two weeks of drought, on 19 May 2015 (T_{drought}), three weeks after rewatering, on 10 June 2015, to evaluate the state of recovery ($T_{\text{recovering}}$), and 16 weeks after rewatering, on 9 September 2015, when new leaves had emerged and were full-grown for several weeks, to assess well-watered reference conditions ($T_{\text{well-watered}}$). Net photosynthesis (P_n) was measured for all fifteen trees on fully matured leaves exposed to the sun, and comparable in size, with a leaf chamber fluorometer (2 cm² leaf area) of a portable photosynthesis system (LI-6400; LI-COR Biosciences, Lincoln, NE, USA). Irradiance was gradually increased from 0 to 2000 $\mu\text{mol m}^{-2} \text{s}^{-1}$ in five steps (0, 50, 100, 1250 and 2000 $\mu\text{mol m}^{-2} \text{s}^{-1}$), each at least lasting 3 min, and leaf gas exchange was determined, while keeping the atmospheric CO₂ concentration at 400 $\mu\text{mol CO}_2 \text{ m}^{-2} \text{s}^{-1}$ and block temperature at 24 °C. All light response curves were measured between 10 h and 16 h. At 0 $\mu\text{mol PAR m}^{-2} \text{s}^{-1}$ the dark respiration rate was measured, and at 2000 $\mu\text{mol PAR m}^{-2} \text{s}^{-1}$ maximum photosynthetic rate was assessed. For all dark respiration measurements, leaves were enclosed in the cuvette for at least 5 min before the actual measurement. Stomatal conductance data were excluded for analysis as the duration of measurements was optimized for light response curves [57].

2.4. Light Response Curves

Light response curves were fitted based on the non-rectangular hyperbola model ([58]; Equation (1)):

$$P_n(I) = \frac{\alpha I + P_{\text{max}} - \sqrt{(\alpha I + P_{\text{max}})^2 - 4I\alpha\theta P_{\text{max}}}}{2\theta} - R_d \quad (1)$$

with $P_n(I)$ ($\mu\text{mol CO}_2 \text{ m}^{-2} \text{s}^{-1}$) the net photosynthetic rate, I the light intensity ($\mu\text{mol PAR m}^{-2} \text{s}^{-1}$), α the initial quantum efficiency ($\mu\text{mol CO}_2 (\mu\text{mol PAR})^{-1}$), P_{max} the maximum gross photosynthetic rate ($\mu\text{mol CO}_2 \text{ m}^{-2} \text{s}^{-1}$), R_d the dark respiration rate ($\mu\text{mol CO}_2 \text{ m}^{-2} \text{s}^{-1}$), and θ the dimensionless or sharpness parameter fixed to a value of 0.5 (e.g., [51,59]). Maximum net photosynthetic rate ($P_{n,\text{max}}$) was calculated by subtracting R_d from P_{max} .

In addition, the light compensation point (I_c) (Equation (2); Fang et al. [58]) and the light saturation point (I_s) at 70% $P_{n,\text{max}}$ ($\delta = P_n/P_{n,\text{max}} = 0.7$) (Equation (3); Wang et al. [49]) were calculated for each measurement day:

$$I_c = \frac{R_d(P_{n,\text{max}} + R_d(1 - \theta))}{\alpha P_{n,\text{max}}} \quad (2)$$

$$L_s = \frac{\delta P_{n,\max}}{\alpha} \left(\frac{\delta - \theta}{1 - \delta} + \theta(1 + \delta) \right) + I_c \quad (3)$$

2.5. $^{11}\text{CO}_2$ Leaf Labeling and Positron Autoradiography

Three reference *M. eminii* trees were taken to INFINITY (INnovative Flemish IN vivo Imaging TechnologY), the pre-clinical imaging lab of Ghent University, Belgium, to carry out ^{11}C -labeling and autoradiography. To avoid disturbance effects caused by transport [55], trees were transported one day before the measurements. A preliminary experiment was performed to assess if tracer transport from leaves to branches still occurred after branch excision. The amount of tracer observed in the branch was similar when comparing cut and uncut branches, and also tracer distribution displayed similar patterns. Two labeling experiments were performed on uncut branches and one on a cut branch. For the latter experiment, a primary branch (~50 cm in length, with 3–5 side-branches) was cut under water to avoid cavitation, shortly before labeling, and was kept in a sealed container with water. In all experiments, the distal end of one of the side-branches (~40 cm in length) was inserted into an air-tight custom-made transparent cylindrical cuvette (20 cm length and 15 cm diameter). A series of red and blue light emitting diodes (LEDs) were positioned inside the cuvette to supply $250 \mu\text{mol PAR m}^{-2} \text{s}^{-1}$ to stimulate photosynthesis. Leaves of the primary branch that remained outside the cuvette were irradiated with a similar PAR intensity. The cuvette was tubed (inner diameter 4.0 mm and outer diameter 5.6 mm) to a LI-6400 (LiCor Biosciences, Lincoln, NE, USA), which provided an inflow ($\pm 0.8 \text{ L min}^{-1}$) with constant humidity and 400 ppm CO_2 concentration, and the outflow was directed to a container with KOH base to trap all $^{11}\text{CO}_2$ exiting the cuvette. The set-up was checked for leakages by ensuring an equal in- and outflow rate. Additionally, the cuvette had a thin inlet tube (inner diameter 0.9 mm and outer diameter 1.5 mm) for administering radioactive $^{11}\text{CO}_2$ isotope tracer gas, with a half-life of 20.4 min. About 370 MBq initial label activity was transferred into the leaf cuvette. During injection, no air flow was present and the leaves were exposed to the tracer for 10 min. Thereafter, air flow was switched on again to remove all $^{11}\text{CO}_2$ from the air surrounding the leaves. The leaves were left in the cuvette for an additional hour before excision and autoradiograph imaging.

^{11}C is an unstable carbon isotope that will emit positrons upon decay. These positrons travel a small distance (on average 1.1 mm, with a maximum of 4 mm, in aqueous medium and much more in air) before colliding with an electron and annihilating into two antiparallel high-energy gamma-rays. Distribution of labeled carbon was imaged by exposing the distal branch part to a multi-sensitive imaging phosphor plate (Perkin Elmer, Waltham, MA, USA), which in case of ^{11}C is mainly sensitive to the emitted positrons. The phosphor plate was positioned on top of the adaxial side of the leaves. Because of the short half-life time of the carbon isotope, fresh samples were used, which implies that we needed to take into account additional factors. Tissue thickness through which positrons must travel can strongly influence their probability of annihilation, which may prevent them of being detected by the autoradiographic plate [60,61]. For autoradiographs, the positron needs to “escape” the leaf in order to be measured by the phosphor screen. The plate was digitally scanned after 10 min exposure using a Cyclone Plus Phosphor imager (Perkin Elmer, Waltham, MA, USA) and OptiQuant software (Perkin Elmer, Waltham, MA, USA). These images were further processed with Fiji, an image processing software [62].

2.6. Stable $\delta^{13}\text{C}$ Isotope Analysis

To determine *M. eminii*'s metabolic pathway for carbon fixation, natural abundance of the stable carbon isotope ^{13}C was measured on a sample of thirty randomly selected old and young $T_{\text{well-watered}}$ leaves. These were pre-weighed and oven-dried at 80°C for five days until constant dry mass was achieved as in [63]. Thereafter, they were ground to fine powder using a ball mill (ZM200, Retsch, Haan, Germany). $\delta^{13}\text{C}$ was determined using an Elemental Analyzer (ANCA-SL, SerCon, Crewe, UK) coupled to an Isotope Ratio Mass Spectrometer (20–20, SerCon, Crewe, UK) (EA-IRMS). Baking

flour with a $\delta^{13}\text{C}$ value of -27.01‰ (certified by IsoAnalytical, Crewe, UK) was used as a laboratory reference, and all $\delta^{13}\text{C}$ are expressed relative to Vienna Pee Dee Belemnite (VPDB).

2.7. Vein Anatomy

Because annihilation probabilities of positrons originating from ^{11}C can be strongly influenced by the amount of overlying tissues, anatomical cross-sections of major veins of the phenologically oldest autoradiographically imaged leaf were analysed. Stored leaf segments, excised in such a way that sections perpendicular to the veins of the first, secondary and tertiary order could be made, were therefore rehydrated overnight in 1% (*v/v*) Aerosol OT (Cytec) and 25% (*v/v*) methanol. After rinsing in demineralised water, samples were embedded in 7% (*w/v*) agarose (Sigma Aldrich, St. Louis, MO, USA). Blocks of agarose containing leaf segments were glued onto the vibratome stage using superglue (Roticoll, Carl Roth). 40 μm thick sections, prepared with a vibrating microtome (HM 650 V, ThermoScientific, Waldorf, Germany), were stained with 0.5% *w/v* astra blue, 0.5% *w/v* chrysoidine and 0.5% *w/v* acridine red and mounted in Euparal after dehydration in isopropyl alcohol. Slides were observed with a Nikon Ni-U microscope (Nikon, Tokyo, Japan) and images were recorded using a Nikon DS-Fi1c camera (Nikon, Tokyo, Japan). Length measurements were performed with Fiji [62] on the cross-section.

2.8. Data Analysis and Statistics

For each set of measurement points a light response curve was fitted according to the non-rectangular hyperbola model. The R^2 was determined to assess the correspondence between measured and modeled data points, and modeled curves with a $R^2 < 0.9$ were not retained for further analysis. This resulted in at least ten light response curves per measurement day used in the analysis. Parameter values were estimated for each individual light response curve and averaged per measurement day. After testing homogeneity of variances (Levene's test, $p > 0.05$), a one-way ANOVA (analysis of variance) was performed, followed by the Tukey's HSD (honest significant difference) post-hoc multiple comparison test, used to analyze significance levels for differences between the three measurement days. For all statistical tests performed, the significance level (P) was set at 5%. Results in text are noted as average \pm standard error.

3. Results

3.1. *M. eminii's* Photosynthetic Performance

Under drought, measured P_{2000} was $2.0 \pm 0.3 \mu\text{mol m}^{-2} \text{s}^{-1}$ ($N = 10$), which more than doubled to $5.0 \pm 0.7 \mu\text{mol m}^{-2} \text{s}^{-1}$ ($N = 10$) under reference conditions ($T_{\text{well-watered}}$) (Figure 1; Table 1). Measured averaged P_{2000} and R_d were both lowest during drought (T_{drought}) (Table 1). In general, relatively large variation was observed between individuals, which reduced the likelihood of measurement differences. Drought $P_{n,\text{max}}$ significantly differed from $P_{n,\text{max}}$ after re-watering, and $P_{n,\text{max}}$ obtained under reference conditions ($T_{\text{drought}} < T_{\text{recovering}} \approx T_{\text{well-watered}}$; $T_{\text{drought}} - T_{\text{recovering}}$ ($p < 0.05$), $T_{\text{drought}} - T_{\text{well-watered}}$ ($p < 0.05$), $T_{\text{recovering}} - T_{\text{well-watered}}$ ($p > 0.05$)). R_d values only significantly differed between drought and three weeks after rewatering ($T_{\text{drought}} - T_{\text{recovering}}$ ($p < 0.001$), $T_{\text{drought}} - T_{\text{well-watered}}$ ($p > 0.05$), $T_{\text{recovering}} - T_{\text{well-watered}}$ ($p > 0.05$)). Initial quantum efficiency (α) reduced under drought ($T_{\text{drought}} - T_{\text{recovering}}$ ($p < 0.05$), $T_{\text{drought}} - T_{\text{well-watered}}$ ($p < 0.05$), $T_{\text{recovering}} - T_{\text{well-watered}}$ ($p > 0.05$)). Other photosynthetic parameters were not significantly affected by drought. Overall, measured light response curves retained for analysis showed close agreement with their corresponding individually fitted non-rectangular hyperbola model (average value of R^2 per fitted curve: T_{drought} ; $R^2 = 0.964$, $T_{\text{recovering}}$; $R^2 = 0.990$, $T_{\text{well-watered}}$; $R^2 = 0.992$). Measured leaves of T_{drought} and $T_{\text{recovering}}$ initially survived the drought treatment, while part of the total leaf mass was shed as immediate response to drought. All leaves that initially survived drought were ultimately shed by the time $T_{\text{well-watered}}$ measurements were carried out. These $T_{\text{well-watered}}$ measurements were performed on newly sprouted leaves, fully mature at the time of measurement.

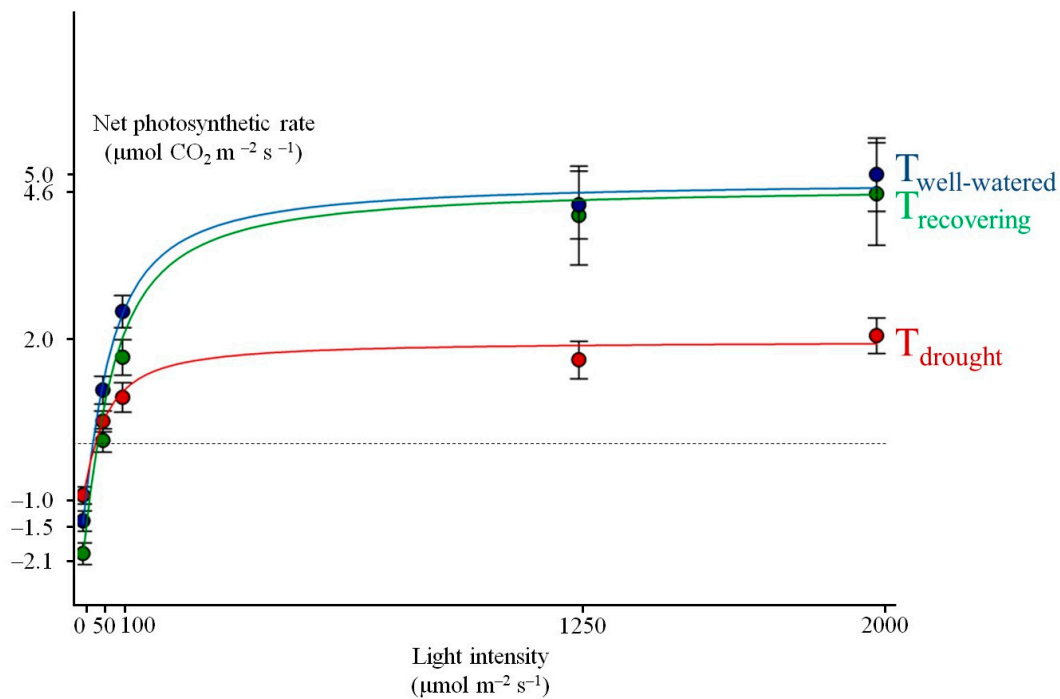


Figure 1. Measured leaf light response curves per potted *Maesopsis eminii* Engl. were individually run in the non-rectangular hyperbola model [58] to obtain average model parameters from which an average light response curve per measurement day was developed. Net photosynthesis (P_n , $\mu\text{mol CO}_2 \text{ m}^{-2} \text{ s}^{-1}$) increases with increasing light intensity (I , $\mu\text{mol m}^{-2} \text{ s}^{-1}$). T_{drought} (after 2 weeks of drought), $T_{\text{recovering}}$ and $T_{\text{well-watered}}$ (respectively, 3 and 16 weeks after rewatering) are depicted in red, green and blue, respectively. Points were obtained by averaging all measurement points of the same measurement day exposed to the same amount of light. Error bars are standard error of the average values (with $N = 10, 12,$ and 10 for $T_{\text{drought}}, T_{\text{recovering}}, T_{\text{well-watered}}$, respectively).

Table 1. Averages of measured and modeled light response curve values per measurement day with standard errors based on N light response curves depicting measured net photosynthetic rate P_{2000} at a light intensity of $2000 \mu\text{mol m}^{-2} \text{ s}^{-1}$ and dark respiration rate R_d values, in addition to non-rectangular hyperbolic model predicted values of P_{2000} , R_d , maximum net photosynthetic rates $P_{n,\text{max}}$, photosynthetic efficiency or slope (α), light saturation point L_s , light compensation point I_c , and R^2 values describing the correlation coefficient between measured points and their individually fitted light response curves. Letters in superscript denote significantly differing values based on a p -value of 0.05.

Measurement Day	Measured Values		Non-Rectangular Hyperbola Model Predicted Values							
	N	P_{2000}	R_d	P_{2000}	R_d	$P_{n,\text{max}}$	α	L_s at 70% $P_{n,\text{max}}$	I_c	R^2
		$\mu\text{mol CO}_2 \text{ m}^{-2} \text{ s}^{-1}$	$\mu\text{mol CO}_2 \text{ m}^{-2} \text{ s}^{-1}$	$\mu\text{mol CO}_2 \text{ m}^{-2} \text{ s}^{-1}$	$\mu\text{mol CO}_2 \text{ m}^{-2} \text{ s}^{-1}$	$\mu\text{mol CO}_2 \text{ m}^{-2} \text{ s}^{-1}$	$(\mu\text{mol PAR})^{-1}$	$\mu\text{mol PAR m}^{-2} \text{ s}^{-1}$		
T_{drought}	10	1.9 ± 0.4^a	1.0 ± 0.1^a	1.8 ± 0.3^a	1.0 ± 0.2^a	1.9 ± 0.3^a	0.042 ± 0.008^a	80 ± 20	50 ± 13	0.964
$T_{\text{recovering}}$	12	4.0 ± 0.9^b	2.0 ± 0.2^b	4.5 ± 1.0^b	2.1 ± 0.2^b	4.8 ± 1.0^b	0.069 ± 0.005^b	71 ± 14	33 ± 6	0.990
$T_{\text{well-watered}}$	10	4.9 ± 0.6^b	$1.4 \pm 0.2^{a,b}$	4.8 ± 0.7^b	$1.5 \pm 0.2^{a,b}$	4.9 ± 0.7^b	0.074 ± 0.009^b	27 ± 7	27 ± 7	0.992

3.2. Estimated Diel Carbon Fluxes and Leaf Carbon Balances

Differences in diel carbon fluxes between drought, recovery and well-watered conditions were assessed by simulating the corresponding photosynthetic rates for a 7-day reference period (using PAR-values of a sunny week from 7 till 13 June 2015 as input in the corresponding light response curves fitted with the non-rectangular hyperbolic model) (Figure 2). Simulated courses were integrated to obtain day- and nighttime as well as total carbon exchange rates (Figure 3). Albeit a simplified approach because fluxes are projected from specific light response curves instead of continuously

measured, it can give a rough estimation of how drought and recovery affect the potential carbon assimilation of leaves. For each water status (i.e., drought, recovery, well-watered), positive daily carbon exchange values were calculated (Figure 3). Significant differences existed between daily carbon exchange after drought and when fully recovered ($T_{\text{drought}} - T_{\text{well-watered}}$, $p < 0.05$). Daily assimilation differed between $T_{\text{drought}} - T_{\text{recovering}}$ ($p < 0.05$), and $T_{\text{drought}} - T_{\text{well-watered}}$ ($p < 0.05$) and nightly respiration differed between $T_{\text{drought}} - T_{\text{recovering}}$ ($p < 0.01$) and $T_{\text{recovering}} - T_{\text{well-watered}}$ ($p \approx 0.05$). Drought-treated leaves lost $34 \pm 10\%$ of their fixed carbon during the day because of nighttime respiration (ratio nighttime respiration and daytime assimilation). Three weeks into recovery, this was $32 \pm 8\%$, but after 16 weeks of rewatering, and being fully recovered, this ratio decreased to $18 \pm 4\%$ (Figure 3).

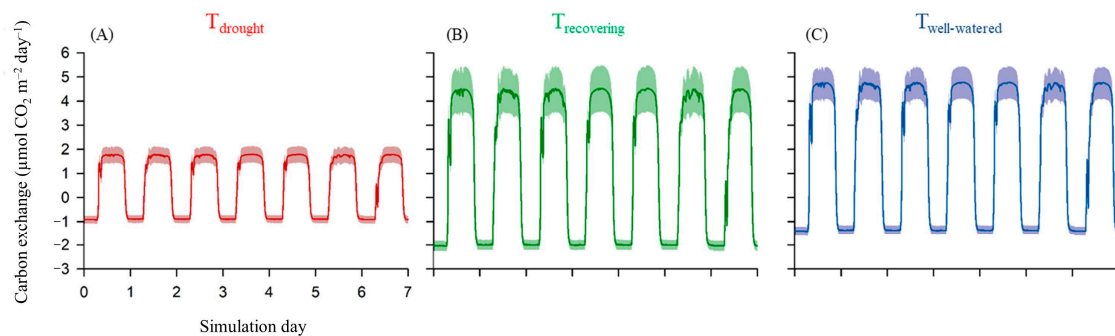


Figure 2. Means of simulated photosynthetic rates ($\mu\text{mol CO}_2 \text{ m}^{-2} \text{ s}^{-1}$) for a 7-day reference week using individual light response curves measured for (A) T_{drought} (red); (B) $T_{\text{recovering}}$ (green) and (C) $T_{\text{well-watered}}$ (blue). Error bands were based on the standard error on the mean of the individually ran simulation curves (with $N = 10, 12$ and 10 for $T_{\text{drought}}, T_{\text{recovering}}, T_{\text{well-watered}}$, respectively).

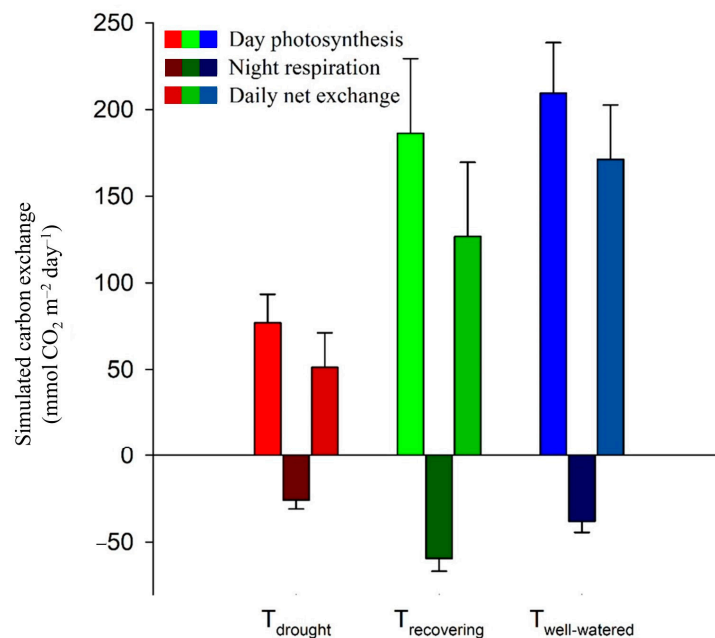


Figure 3. Conversion of simulated photosynthetic rates (Figure 2) into leaf carbon exchange represented as night respiration and daytime photosynthesis, and yielding daily net carbon uptake. Error bars were obtained as standard error of the means ($N = 10, 12$, and 10 for $T_{\text{drought}}, T_{\text{recovering}}, T_{\text{well-watered}}$, respectively) from the individually ran simulation curves in Figure 2.

3.3. ^{11}C Autoradiographs and ^{13}C Stable Isotope

Autoradiographs displayed a high correspondence with venation (Figure 4). In younger leaves, the signal is nearly equally distributed across the leaf blade, whereas in the older leaves the signal accumulated more around the primary and secondary veins. Tracer detection in the veins was lower, which may be attributed to a higher amount of annihilations taking place in the thicker layer of overlying tissues present in the major veins.



Figure 4. Positron autoradiographs of *Maesopsis eminii* leaves from the distal end of a secondary branch arranged from younger to older (left to right) leaves, showing the distribution of ^{11}C , 1 h after $^{11}\text{CO}_2$ was administered to an excised branch. The adaxial side of the leaves was exposed to the phosphor plate. Brighter regions reflect higher ^{11}C accumulation. Younger leaves have a uniform carbon distribution across the leaf blade, while older leaves show a higher accumulation around the primary and secondary veins. Some leaves show larger areas that are less bright, which is attributed to shading of these areas by other leaves.

M. eminii's stable carbon isotope signature ($\delta^{13}\text{C}$) was $-27.8 \pm 0.2\text{‰}$ ($N = 20$), pointing to C_3 -metabolism [64].

3.4. Anatomy of the Main, Secondary and Tertiary Veins

Vascular bundles of the main and secondary veins were located above halfway the leaf cross-section, whereas in tertiary veins these were found below halfway the section (Figure 5). Secondary veins showed a layer of parenchymatic cells beneath the vascular bundle, whereas an entire parenchymatic bundle sheath was observed around tertiary veins. These parenchyma cells did not contain chloroplasts. Leaf thickness was measured to assess the effect of increased probability of annihilation when moving from smaller to larger veins. Distances were measured between points in the vascular bundle and the adaxial side of the leaf (i.e., the side that was exposed to the phosphor plate) to derive average distances that positrons had to travel before reaching the phosphor plate. These distances were $206 \pm 23 \mu\text{m}$, $88.0 \pm 5.4 \mu\text{m}$, and $67.41 \pm 0.92 \mu\text{m}$ ($N = 8$ each) for the main, secondary and tertiary vein, respectively. Leaf thickness was on average $123 \pm 14 \mu\text{m}$ ($N = 12$). For the mesophyll it is uncertain where in the leaf ^{11}C would be mainly found. Probably, most is found in the photosynthetically active palisade cells close to the adaxial side. Average distance between palisade cells and the adaxial edge of the leaf was $28.0 \pm 2.4 \mu\text{m}$ ($N = 8$). When assuming ^{11}C tracer to be positioned in the palisade tissue when in the mesophyll, and in the vascular bundle when in the veins, the reduction in positron escape and thus detected signal can be calculated, according to [36]. Following this approach, a reduction in detected signal of 3%, 4% and 12% was calculated for tertiary, secondary and primary veins, respectively. These corrections should be used indicatively, but when applied, resulted in similar intensities in the major veins and in the adjacent tissue (Figure 4).

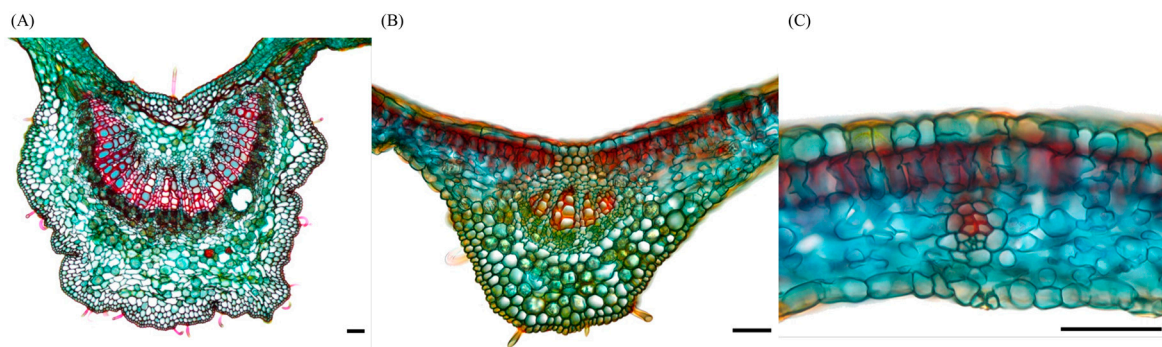


Figure 5. Anatomical cross-section of (A) the major vein; (B) a secondary vein and (C) a tertiary vein from the oldest autoradiographically imaged leaf in Figure 4. A parenchymatic layer is visible under the vascular bundle of the secondary vein and a parenchymatic sheath around the tertiary vein. Images were used to determine the distance between the phloem in the vascular bundle and the adaxial side of the leaf (top of the image), which was exposed to the phosphor screen for autoradiography. Scale bar is 50 μm .

4. Discussion

As expected, drought lowered *M. eminii*'s average reference $P_{n,\text{max}}$ (by 60%, Figure 1; Table 1). Koller et al. [65] reported a similar reduction in photosynthesis of about 60% after three weeks of withholding water in three evergreen *Quercus* spp. comparable in height with our study trees. Varone et al. [66] investigated several Mediterranean species and observed a photosynthetic reduction of 50% in less than a week after imposing drought. This reduction in photosynthesis is usually linked with stomatal closure in response to a depleting soil water status (e.g., [29,30,65,67–70]).

Three weeks into re-watering ($T_{\text{recovering}}$) *M. eminii* reached $P_{n,\text{max}}$ values similar to those of the well-watered reference period ($T_{\text{well-watered}}$), but R_d was considerably higher, indicating a metabolic cost for recovery (Figure 1, Table 1). The high R_d values measured after three weeks of recovery can be attributed to a biphasic response, which occurs in some species [30]. During drought, $P_{n,\text{max}}$ decreased, accompanied by a decrease in R_d , as is observed in many species. After rewatering, leaves needed to recover from the negative drought-induced effects. This increased the energy demand for maintenance and repair, resulting in higher respiration rates [29,30]. Higher respiratory rates can also indicate higher vulnerability to drought as was observed by Peguero-Pina et al. [71] in Mediterranean oaks. In their study, *Quercus suber* L. showed higher respiratory rates than *Q. coccifera* L. and *Q. ilex* ssp. *ballota* (Desf.) Samp under intense drought, with data suggesting that *Q. suber* was less able to withstand highly xeric conditions. *M. eminii* leaves showed higher respiratory rates during drought recovery, but in the long run all leaves that had experienced drought were shed, indicating that these leaves were susceptible to drought. Resprouting of new leaf material occurred shortly after rewatering, which might be a more efficient strategy: trading drought-stressed leaves with high respiratory demands (R_d in $T_{\text{recovering}}$) through leaf shedding, for new leaves with lower respiratory demands (R_d in $T_{\text{well-watered}}$). The ecological significance of drought-deciduousness or evergreenness strongly depends on the prevailing climate, with climate change being expected to induce a shift towards drought-deciduous communities [41].

Measurements of photosynthetic rates in pioneers typically yield high $P_{n,\text{max}}$ values under well-watered conditions. Despite its pioneering trait, *M. eminii* showed relatively low $P_{n,\text{max}}$ values ($5.0 \pm 0.7 \mu\text{mol m}^{-2} \text{s}^{-1}$; Figure 1, Table 1). Earlier greenhouse studies on tropical pioneer species reported typical $P_{n,\text{max}}$ values of $10 \mu\text{mol m}^{-2} \text{s}^{-1}$ and higher, which is substantially higher than *M. eminii*'s $P_{n,\text{max}}$ (e.g., [72–74]). Also field measurements of $P_{n,\text{max}}$ in tropical pioneers are typically higher than *M. eminii*'s values. In their photosynthetic study on several tree species in the Cameroonian rainforest, Meir et al. [75] found pioneers to have $P_{n,\text{max}}$ values within the range $6\text{--}13 \mu\text{mol CO}_2 \text{m}^{-2} \text{s}^{-1}$. An older study in a Nigerian rainforest reported photosynthetic rates of

about 5–7 $\mu\text{mol CO}_2 \text{ m}^{-2} \text{ s}^{-1}$, and although measured at lower PAR-levels (around 800 $\mu\text{mol m}^{-2} \text{ s}^{-1}$), this study indicates that other tropical pioneer species also may show low P_n values [76]. In Panama, Ellis et al. [77] conducted a study on a variety of tropical trees to conclude that pioneer species had significantly higher $P_{n,\text{max}}$ values compared to non-pioneer species with an average $P_{n,\text{max}}$ of 16 $\mu\text{mol CO}_2 \text{ m}^{-2} \text{ s}^{-1}$. Another study conducted by Domingues et al. [78] in an African savanna and semi-deciduous dry forest reported values higher than 7 $\mu\text{mol CO}_2 \text{ m}^{-2} \text{ s}^{-1}$. Despite its relatively low P_n and high R_d rates, *M. eminii* was simulated to be a carbon sink during all conditions (Figures 2 and 3).

Current vegetation models typically use photosynthesis as a determinant for plant growth [22]. Our results suggest a potential mismatch between leaf photosynthetic rates and the pioneering, fast-growing behavior of *M. eminii*. Fatichi et al. [22] discussed possible elements causing the decoupling between photosynthesis and growth rates, including the effects of nutrient availability, meristematic processes, the role of carbon reserves (accumulation and depletion of non-structural carbon pools) or the multiple impacts of water on many physiological processes [38]. Not only source activity determines plant growth, but entire source-sink relationships need to be considered [22]. *M. eminii*'s behavior during dry conditions in terms of substantial stem water storage and buffered water potentials might explain its ability to sustain high growth rate despite the measured low photosynthetic rates [42].

As a woody tree species, *M. eminii* was found to be C_3 ($-27.8 \pm 0.2\text{‰}$) in nature, with C_3 plants having a $\delta^{13}\text{C}$ range of -21 to -35‰ , and C_4 from -9 to -20‰ [64]. Pulse-labeling experiments with both $^{11}\text{CO}_2$ and $^{14}\text{CO}_2$ on leaves have been performed in the past, but mainly focused on quantification of the continuous export of label out of the leaf. In this study, we focused on imaging tracer distribution inside the leaf, relatively shortly after labeling (one hour) [79–81]. $^{11}\text{CO}_2$ pulse-labeling performed by Jahnke et al. [80] on young *Fraxinus excelsior* L. and *Sorbus aucuparia* L. trees showed a continuous and constant export of carbon tracer out of the leaves for at least two hours. Based on these observations, it was assumed that *M. eminii* exports carbon at a constant rate between the time of pulse-labeling and imaging. Under such steady-state conditions, autoradiographic carbon patterns display carbon distribution inside the leaf. Commonly, trees use a passive loading strategy, characterized by a higher concentration of sugars in the mesophyll and a lower concentration in the veins (e.g., [32,40,82,83]). Previous ^{14}C labeling experiments have evaluated loading strategies of species and reported that active loaders showed higher tracer accumulation in the veins and passive loaders in the mesophyll [32,82,83]. In older leaves of *M. eminii*, tracer intensity was elevated near the main and secondary veins, whereas in active loaders a higher presence of tracer is expected inside the veins. With our approach of using fresh leaf material and ^{11}C , quantification of tracer activity is complicated by the difference in thickness between main and secondary veins in comparison to mesophyll, and potential differences in water content. The layers overlying the major veins reduce the amount of detected tracer signal (Figure 5), explaining why major veins are less bright on the autoradiographs. After tissue thickness correction, the same tracer accumulation was observed as in the brighter adjacent tissue (Figure 4). A distinct difference in tracer amount was found in the mesophyll with an accumulation pattern directed towards the major veins. According to studies by Rennie and Turgeon [82] and Fu et al. [83] this indicates an active loading strategy. Alternatively, this distribution pattern could be due to rapid export of tracer out of the mesophyll, with most of the tracer already within the major veins after pulse-labeling, which still indicates active loading. $^{14}\text{CO}_2$ autoradiographs of *Nicotiana tabacum* L., an active loader with high export rates, also showed elevated tracer amounts in the major veins, with a lower evenly distributed amount of tracer in the mesophyll, measured one hour after labeling [84]. The active phloem loading strategy has been linked to (i) an increased carbon export from leaves to sinks (e.g., shoots and roots) [32,40,85]; (ii) an improved efficiency of sugar transport [58]; and (iii) an increased growth potential [40]. Active transport is less common in woody tree species, but not unique [83]. Turgeon [40] investigated why active loading is commonly found in herbaceous species, and passive loading in tree species. He concluded that continuous investment in growth by herbaceous species favored active loading while passive loading is more favorable for trees that require investment in storage inventories

used during leafless periods (e.g., in winter) and growth flushes. *M. eminii*, like many tropical species, is only deciduous in response to drought [86], which is also a common trait for herbaceous species. According to Turgeon [40], the lower leaf carbon inventory of active loaders has a significant effect on the plant's growth potential, which might explain *M. eminii*'s low photosynthetic rate but rapid growth. As in the tropics most trees are drought-deciduous or evergreen, more research on how tropical tree species load carbohydrates into the phloem is warranted. Large studies investigating phloem loading strategies show that available data on tropical species is limited [79,80,83]. Younger leaves in our study showed a relatively uniform tracer distribution throughout the mesophyll (Figure 4). Since thickness effect on positron annihilation probability can be ignored in thin objects, such as young leaves with thin veins, their distribution pattern might indicate passive sugar loading into the phloem, or import of tracer from the older leaves, because young leaves are often net carbon importers, rather than exporters [70].

5. Conclusions

M. eminii is a pioneer with fast growth, expected to show a high photosynthetic rate, but this was not confirmed by our measurements. The mismatch between photosynthesis and growth indicated that *M. eminii* might use other features to obtain fast growth. ^{11}C -autoradiographic tracer patterns in mature leaves suggested an active phloem loading strategy, which can be related to fast growth. This study hence illustrated that, besides photosynthesis, photoassimilate distribution and phloem loading may be important in the assessment of leaf and tree carbon balances. This has been previously acknowledged by Fatichi et al. [22], and highlights the need for more measurements, which will pave the way for a better understanding of the ecophysiology of tropical trees. This is necessary if we aspire to predict how tropical trees and forests will cope with climatic changes and how this will feedback to global carbon and water cycling (e.g., [38,82,83,87,88]).

Acknowledgments: We would like to thank Olivier Leroux, for his skillful work on the anatomical cross-sections. Sincere gratitude also goes to Christian Vanhove, Benedicte Descamps, Jan Courty, Boudewijn Brans and Jens Mincke for assisting with the ^{11}C labeling and autoradiographs, and to Stefan Vidts, Geert Favys, Ingvar Bauweraerts, Jonas Coussement and Thomas Van De Putte for their help during the greenhouse measurements. A special thanks goes to Michael Thorpe for providing useful insights into ^{11}C autoradiography, which helped in putting the results into a good perspective. Comments from three reviewers further improved the quality of the manuscript. Funding: Flemish Interuniversity Council/VLIR-OUS (ICP Ph.D. 2012-001 granted to J.E.), Research Foundation—Flanders (FWO) (G.0319.13N granted to K.S.) and Flanders Innovation & Entrepreneurship (141660 granted to M.H.).

Author Contributions: K.S. conceptualized the experimental setups, and assisted in data interpretation and writing of the manuscript. J.E. and M.H. carried out the experiments, analyzed, interpreted the data, and wrote the manuscript. All authors critically revised the manuscript and approve the final version to be published.

Conflicts of Interest: The authors declare no conflict of interest.

References

1. IPCC. Summary for Policymakers. In *Climate Change 2013: The Physical Science Basis. Contribution of Working Group I to the Fifth Assessment Report of the Intergovernmental Panel on Climate Change*; Stocker, T.F., Qin, D., Plattner, G.-K., Tignor, M., Allen, S.K., Boschung, J., Nauels, A., Xia, Y., Bex, V., Midgley, P.M., Eds.; Cambridge University Press: Cambridge, UK; New York, NY, USA, 2013; pp. 3–29.
2. Fauset, S.; Baker, T.R.; Lewis, S.L.; Feldpausch, T.R.; Affum-Baffoe, K.; Foli, E.G.; Hamer, K.C.; Swaine, M.D. Drought-induced shifts in the floristic and functional composition of tropical forests in Ghana. *Ecol. Lett.* **2012**, *15*, 1120–1129. [[CrossRef](#)] [[PubMed](#)]
3. Asefi-Najafabady, S.; Saatchi, S. Response of African humid tropical forests to recent rainfall anomalies. *Philos. Trans. R. Soc. B* **2013**, *368*, 20120306. [[CrossRef](#)] [[PubMed](#)]
4. James, R.; Washington, R.; Rowell, D.P. Implications of global warming for the climate of African rainforests. *Philos. Trans. R. Soc. B* **2013**, *368*, 20120298. [[CrossRef](#)] [[PubMed](#)]
5. Malhi, Y.; Adu-Bredu, S.; Asare, R.A.; Lewis, S.L.; Mayaux, P. African rainforests: Past, present and future. *Philos. Trans. R. Soc. B* **2013**, *368*, 20120312. [[CrossRef](#)] [[PubMed](#)]

6. Oslisly, R.; White, L.; Bentaleb, I.; Favier, C.; Fontugne, M.; Gillet, J.-F.; Sebag, D. Climatic and cultural changes in the west congo basin forests over the past 5000 years. *Philos. Trans. R. Soc. B* **2013**, *368*, 20120304. [[CrossRef](#)] [[PubMed](#)]
7. Otto, F.E.; Jones, R.G.; Halladay, K.; Allen, M.R. Attribution of changes in precipitation patterns in African rainforests. *Philos. Trans. R. Soc. B* **2013**, *368*, 20120299. [[CrossRef](#)] [[PubMed](#)]
8. Ouédraogo, D.Y.; Mortier, F.; Gourlet-Fleury, S.; Freycon, V.; Picard, N. Slow-growing species cope best with drought: Evidence from long-term measurements in a tropical semi-deciduous moist forest of Central Africa. *J. Ecol.* **2013**, *101*, 1459–1470. [[CrossRef](#)]
9. Willis, K.; Bennett, K.D.; Burrough, S.; Macias-Fauria, M.; Tovar, C. Determining the response of African biota to climate change: Using the past to model the future. *Philos. Trans. R. Soc. B* **2013**, *368*, 20120491. [[CrossRef](#)] [[PubMed](#)]
10. Zhou, L.; Tian, Y.; Myneni, R.B.; Ciais, P.; Saatchi, S.; Liu, Y.Y.; Piao, S.; Chen, H.; Vermote, E.F.; Song, C. Widespread decline of congo rainforest greenness in the past decade. *Nature* **2014**, *509*, 86–90. [[CrossRef](#)] [[PubMed](#)]
11. Williams, C.A.; Hanan, N.P.; Neff, J.C.; Scholes, R.J.; Berry, J.A.; Denning, A.S.; Baker, D.F. Africa and the global carbon cycle. *Carbon Balance Manag.* **2007**, *2*, 3. [[CrossRef](#)] [[PubMed](#)]
12. Fisher, J.B.; Sikka, M.; Sitch, S.; Ciais, P.; Poulter, B.; Galbraith, D.; Lee, J.E.; Huntingford, C.; Viovy, N.; Zeng, N. African tropical rainforest net carbon dioxide fluxes in the twentieth century. *Philos. Trans. R. Soc. B* **2013**, *368*, 20120376. [[CrossRef](#)] [[PubMed](#)]
13. Cao, M.; Zhang, Q.; Shugart, H.H. Dynamic responses of African ecosystem carbon cycling to climate change. *Clim. Res.* **2001**, *17*, 183–193. [[CrossRef](#)]
14. McGuire, A.; Sitch, S.; Klein, J.; Dargaville, R.; Esser, G.; Foley, J.; Heimann, M.; Joos, F.; Kaplan, J.; Kicklighter, D.W.; et al. Carbon balance of the terrestrial biosphere in the twentieth century: Analyses of CO₂, climate and land use effects with four process-based ecosystem models. *Glob. Biogeochem. Cycles* **2001**, *15*, 183–206. [[CrossRef](#)]
15. Ciais, P.; Piao, S.-L.; Cadule, P.; Friedlingstein, P.; Chédin, A. Variability and recent trends in the African terrestrial carbon balance. *Biogeosciences* **2009**, *6*, 1935–1948. [[CrossRef](#)]
16. Hiernaux, P.; Mougin, E.; Diarra, L.; Soumaguel, N.; Lavenu, F.; Tracol, Y.; Diawara, M. Sahelian rangeland response to changes in rainfall over two decades in the gourma region, Mali. *J. Hydrol.* **2009**, *375*, 114–127. [[CrossRef](#)]
17. Lewis, S.L.; Lopez-Gonzalez, G.; Sonké, B.; Affum-Baffoe, K.; Baker, T.R.; Ojo, L.O.; Phillips, O.L.; Reitsma, J.M.; White, L.; Comiskey, J.A. Increasing carbon storage in intact African tropical forests. *Nature* **2009**, *457*, 1003–1006. [[CrossRef](#)] [[PubMed](#)]
18. Ciais, P.; Bombelli, A.; Williams, M.; Piao, S.; Chave, J.; Ryan, C.; Henry, M.; Brender, P.; Valentini, R. The carbon balance of Africa: Synthesis of recent research studies. *Philos. Trans. R. Soc. B* **2011**, *369*, 2038–2057. [[CrossRef](#)] [[PubMed](#)]
19. Washington, R.; James, R.; Pearce, H.; Pokam, W.M.; Moufouma-Okia, W. Congo basin rainfall climatology: Can we believe the climate models? *Philos. Trans. R. Soc. B* **2013**, *368*, 20120296. [[CrossRef](#)] [[PubMed](#)]
20. DosAnjos, L.; Oliva, M.A.; Kuki, K.N.; Mielke, M.S.; Ventrella, M.C.; Galvão, M.F.; Pinto, L.R. Key leaf traits indicative of photosynthetic plasticity in tropical tree species. *Trees* **2015**, *29*, 247–258. [[CrossRef](#)]
21. Atkin, O.K.; Bloomfield, K.J.; Reich, P.B.; Tjoelker, M.G.; Asner, G.P.; Bonal, D.; Bönisch, G.; Bradford, M.G.; Cernusak, L.A.; Cosio, E.G. Global variability in leaf respiration in relation to climate, plant functional types and leaf traits. *New Phytol.* **2015**, *206*, 614–636. [[CrossRef](#)] [[PubMed](#)]
22. Fatichi, S.; Leuzinger, S.; Körner, C. Moving beyond photosynthesis: From carbon source to sink-driven vegetation modeling. *New Phytol.* **2014**, *201*, 1086–1095. [[CrossRef](#)] [[PubMed](#)]
23. Doughty, C.E.; Metcalfe, D.; Girardin, C.; Amézquita, F.F.; Cabrera, D.G.; Huasco, W.H.; Silva-Espejo, J.; Araujo-Murakami, A.; da Costa, M.; Rocha, W. Drought impact on forest carbon dynamics and fluxes in Amazonia. *Nature* **2015**, *519*, 78–82. [[CrossRef](#)] [[PubMed](#)]
24. Malhi, Y.; Doughty, C.E.; Goldsmith, G.R.; Metcalfe, D.B.; Girardin, C.A.; Marthews, T.R.; Aguila-Pasquel, J.; Aragão, L.E.; Araujo-Murakami, A.; Brando, P. The linkages between photosynthesis, productivity, growth and biomass in lowland Amazonian forests. *Glob. Chang. Biol.* **2015**, *21*, 2283–2295. [[CrossRef](#)] [[PubMed](#)]

25. Kearsley, E.; de Haulleville, T.; Hufkens, K.; Kidimbu, A.; Toirambe, B.; Baert, G.; Huygens, D.; Kebede, Y.; Defourny, P.; Bogaert, J. Conventional tree height-diameter relationships significantly overestimate aboveground carbon stocks in the central congo basin. *Nat. Commun.* **2013**, *4*. [[CrossRef](#)] [[PubMed](#)]
26. Chave, J.; Réjou-Méchain, M.; Búrquez, A.; Chidumayo, E.; Colgan, M.S.; Delitti, W.B.; Duque, A.; Eid, T.; Fearnside, P.M.; Goodman, R.C. Improved allometric models to estimate the aboveground biomass of tropical trees. *Glob. Chang. Biol.* **2014**, *20*, 3177–3190. [[CrossRef](#)] [[PubMed](#)]
27. Picard, N.; Henry, M.; Fonton, N.H.; Kondaoulé, J.; Fayolle, A.; Birigazzi, L.; Sola, G.; Poultouchidou, A.; Trotta, C.; Maïdou, H. Error in the estimation of emission factors for forest degradation in central Africa. *J. For. Res.* **2016**, *21*, 23–30. [[CrossRef](#)]
28. Saatchi, S.; Mascaró, J.; Xu, L.; Keller, M.; Yang, Y.; Duffy, P.; Espírito-Santo, F.; Baccini, A.; Chambers, J.; Schimel, D. Seeing the forest beyond the trees. *Glob. Ecol. Biogeogr.* **2015**, *24*, 606–610. [[CrossRef](#)]
29. Flexas, J.; Bota, J.; Galmes, J.; Medrano, H.; Ribas-Carbó, M. Keeping a positive carbon balance under adverse conditions: Responses of photosynthesis and respiration to water stress. *Physiol. Plant.* **2006**, *127*, 343–352. [[CrossRef](#)]
30. Flexas, J.; Galmes, J.; Ribas-Carbo, M.; Medrano, H. The effects of water stress on plant respiration. In *Plant Respiration*; Lambers, H., Ribas-Carbo, M., Eds.; Springer: Dordrecht, The Netherlands, 2005; pp. 85–94.
31. Varone, L.; Gratani, L. Leaf respiration responsiveness to induced water stress in Mediterranean species. *Environ. Exp. Bot.* **2015**, *109*, 141–150. [[CrossRef](#)]
32. De Schepper, V.; Bühler, J.; Thorpe, M.; Roeb, G.; Huber, G.; van Dusschoten, D.; Jahnke, S.; Steppe, K. ¹¹C-pet imaging reveals transport dynamics and sectorial plasticity of oak phloem after girdling. *Front. Plant Sci.* **2013**, *4*, 200. [[CrossRef](#)] [[PubMed](#)]
33. Mencuccini, M. Temporal scales for the coordination of tree carbon and water economies during droughts. *Tree Physiol.* **2014**, *34*, 439–442. [[CrossRef](#)] [[PubMed](#)]
34. Sevanto, S. Phloem transport and drought. *J. Exp. Bot.* **2014**, *65*, 1751–1759. [[CrossRef](#)] [[PubMed](#)]
35. Hubeau, M.; Steppe, K. Plant-PET scans: In vivo mapping of xylem and phloem functioning. *Trends Plant Sci.* **2015**, *20*, 676–685. [[CrossRef](#)] [[PubMed](#)]
36. Steppe, K.; Sterck, F.; Deslauriers, A. Diel growth dynamics in tree stems: Linking anatomy and ecophysiology. *Trends Plant Sci.* **2015**, *20*, 335–343. [[CrossRef](#)] [[PubMed](#)]
37. Ryan, M.G.; Hubbard, R.M.; Pongracic, S.; Raison, R.; McMurtrie, R.E. Foliage, fine-root, woody-tissue and stand respiration in *Pinus radiata* in relation to nitrogen status. *Tree Physiol.* **1996**, *16*, 333–343. [[CrossRef](#)] [[PubMed](#)]
38. Van der Molen, M.K.; Dolman, A.J.; Ciais, P.; Eglin, T.; Gobron, N.; Law, B.E.; Meir, P.; Peters, W.; Phillips, O.L.; Reichstein, M.; et al. Drought and ecosystem carbon cycling. *Agric. For. Meteorol.* **2011**, *151*, 765–773. [[CrossRef](#)]
39. Gustafson, E.J.; De Bruijn, A.M.; Pangle, R.E.; Limousin, J.M.; McDowell, N.G.; Pockman, W.T.; Sturtevant, B.R.; Muss, J.D.; Kubiske, M.E. Integrating ecophysiology and forest landscape models to improve projections of drought effects under climate change. *Glob. Chang. Biol.* **2015**, *21*, 843–856. [[CrossRef](#)] [[PubMed](#)]
40. Turgeon, R. The role of phloem loading reconsidered. *Plant Physiol.* **2010**, *152*, 1817–1823. [[CrossRef](#)] [[PubMed](#)]
41. Vico, G.; Dralle, D.; Feng, X.; Thompson, S.; Manzoni, S. How competitive is drought deciduousness in tropical forests? A combined eco-hydrological and eco-evolutionary approach. *Environ. Res. Lett.* **2017**, *12*, 065006. [[CrossRef](#)]
42. Epila, J.; Maes, W.H.; Verbeeck, H.; Van Camp, J.; Okullo, J.B.L.; Steppe, K. Plant measurements on African tropical *Maesopsis eminii* seedlings contradict pioneering water use behaviour. *Environ. Exp. Bot.* **2017**, *135*, 27–37. [[CrossRef](#)]
43. Van Camp, J.; Hubeau, M.; Van den Bulcke, J.; Van Acker, J.; Steppe, K. Cambial pinning relates wood anatomy to ecophysiology in the African tropical tree *Maesopsis eminii*. *Tree Physiol.* **2018**, *38*, 232–242. [[CrossRef](#)] [[PubMed](#)]
44. Caird, M.A.; Richards, J.H.; Donovan, L.A. Nighttime stomatal conductance and transpiration in C₃ and C₄ plants. *Plant Physiol.* **2007**, *143*, 4–10. [[CrossRef](#)] [[PubMed](#)]
45. Chen, X.; Gao, J.; Zhao, P.; McCarthy, H.R.; Zhu, L.; Ni, G.; Ouyang, L. Tree species with photosynthetic stems have greater nighttime sap flux. *Front. Plant Sci.* **2018**, *9*, 30. [[CrossRef](#)] [[PubMed](#)]

46. Epila, J.; De Baerdemaeker, N.J.F.; Vergeynst, L.L.; Maes, W.H.; Beeckman, H.; Steppe, K. Capacitive water release and internal leaf water relocation delay drought-induced cavitation in African *Maesopsis emini*. *Tree Physiol.* **2017**, *37*, 481–490.
47. Tyree, M.T.; Engelbrecht, B.M.; Vargas, G.; Kursar, T.A. Desiccation tolerance of five tropical seedlings in Panama. Relationship to a field assessment of drought performance. *Plant Physiol.* **2003**, *132*, 1439–1447. [[PubMed](#)]
48. Engelbrecht, B.M.; Kursar, T.A.; Tyree, M.T. Drought effects on seedling survival in a tropical moist forest. *Trees* **2005**, *19*, 312–321. [[CrossRef](#)]
49. Wang, K.; Kellomäki, S.; Laitinen, K. Effects of needle age, long-term temperature and CO₂ treatments on the photosynthesis of scots pine. *Tree Physiol.* **1995**, *15*, 211–218. [[CrossRef](#)] [[PubMed](#)]
50. Cannell, M.; Thornley, J. Temperature and CO₂ responses of leaf and canopy photosynthesis: A clarification using the non-rectangular hyperbola model of photosynthesis. *Ann. Bot.* **1998**, *82*, 883–892. [[CrossRef](#)]
51. Thornley, J. Dynamic model of leaf photosynthesis with acclimation to light and nitrogen. *Ann. Bot.* **1998**, *81*, 421–430. [[CrossRef](#)]
52. Epron, D.; Bahn, M.; Derrien, D.; Lattanzi, F.A.; Pumpanen, J.; Gessler, A.; Hogberg, P.; Maillard, P.; Dannoura, M.; Gerant, D.; et al. Pulse-labelling trees to study carbon allocation dynamics: A review of methods, current knowledge and future prospects. *Tree Physiol.* **2012**, *32*, 776–798. [[CrossRef](#)] [[PubMed](#)]
53. Zuidema, P.A.; Baker, P.J.; Groenendijk, P.; Schippers, P.; van der Sleen, P.; Vlam, M.; Sterck, F. Tropical forests and global change: Filling knowledge gaps. *Trends Plant Sci.* **2013**, *18*, 413–419. [[CrossRef](#)] [[PubMed](#)]
54. Kiser, M.R.; Reid, C.D.; Crowell, A.S.; Phillips, R.P.; Howell, C.R. Exploring the transport of plant metabolites using positron emitting radiotracers. *HFSP J.* **2008**, *2*, 189–204. [[CrossRef](#)] [[PubMed](#)]
55. Minchin, P.E.H.; Thorpe, M.R. Using the short-lived isotope ¹¹C in mechanistic studies of photosynthate transport. *Funct. Plant Biol.* **2003**, *30*, 831–841. [[CrossRef](#)]
56. Bloemen, J.; Bauweraerts, I.; De Vos, F.; Vanhove, C.; Vandenberghe, S.; Boeckx, P.; Steppe, K. Fate of xylem-transported ¹¹C- and ¹³C-labeled CO₂ in leaves of poplar. *Physiol. Plant.* **2015**, *153*, 555–564. [[CrossRef](#)] [[PubMed](#)]
57. LI-CO. *Using the LI-6400/LI-6400XT Portable Photosynthesis System*; LI-COR: Lincoln, NE, USA, 2008.
58. Fang, L.; Zhang, S.; Zhang, G.; Liu, X.; Xia, X.; Zhang, S.; Xing, W.; Fang, X. Application of five light-response models in the photosynthesis of *populus × euramericana* cv. ‘Zhonglin46’ leaves. *Appl. Biochem. Biotechnol.* **2015**, *176*, 86–100. [[CrossRef](#)] [[PubMed](#)]
59. Calama, R.; Puértolas, J.; Madrigal, G.; Pardos, M. Modeling the environmental response of leaf net photosynthesis in *Pinus pinea* L. Natural regeneration. *Ecol. Model.* **2013**, *251*, 9–21. [[CrossRef](#)]
60. Levin, C.S.; Hoffman, E.J. Calculation of positron range and its effect on the fundamental limit of positron emission tomography system spatial resolution. *Phys. Med. Biol.* **1999**, *44*, 781–799. [[CrossRef](#)] [[PubMed](#)]
61. Jødal, L.; Le Loirec, C.; Champion, C. Positron range in PET imaging: An alternative approach for assessing and correcting the blurring. *Phys. Med. Biol.* **2012**, *57*, 3931. [[CrossRef](#)] [[PubMed](#)]
62. Schindelin, J.; Arganda-Carreras, I.; Frise, E.; Kaynig, V.; Longair, M.; Pietzsch, T.; Preibisch, S.; Rueden, C.; Saalfeld, S.; Schmid, B. Fiji: An open-source platform for biological-image analysis. *Nat. Methods* **2012**, *9*, 676–682. [[CrossRef](#)] [[PubMed](#)]
63. Ehleringer, J.R. ¹³C/¹²C fractionation and its utility in terrestrial plant studies. In *Carbon Isotope Techniques*; Coleman, D.C., Fry, B., Eds.; Academic Press: San Diego, CA, USA, 1991; pp. 187–200.
64. O’Leary, M.H. Carbon isotopes in photosynthesis. *Bioscience* **1988**, *38*, 328–336. [[CrossRef](#)]
65. Koller, S.; Holland, V.; Brüggemann, W. Effects of drought stress on the evergreen *Quercus ilex* L., the deciduous *Q. robur* L. And their hybrid *Q. × turneri* willd. *Photosynthetica* **2013**, *51*, 574–582. [[CrossRef](#)]
66. Varone, L.; Ribas-Carbo, M.; Cardona, C.; Gallé, A.; Medrano, H.; Gratani, L.; Flexas, J. Stomatal and non-stomatal limitations to photosynthesis in seedlings and saplings of Mediterranean species pre-conditioned and aged in nurseries: Different response to water stress. *Environ. Exp. Bot.* **2012**, *75*, 235–247. [[CrossRef](#)]
67. Loustalot, A.J. Influence of soil moisture conditions on apparent photosynthesis and transpiration of pecan leaves. *J. Agric. Res.* **1945**, *71*, 519–532.
68. Upchurch, R.P.; Peterson, M.L.; Hagan, R.M. Effect of soil-moisture content on the rate of photosynthesis and respiration in ladino clover (*Trifolium repens* L.). *Plant Physiol.* **1995**, *30*, 297–303. [[CrossRef](#)]

69. De Swaef, T.; Steppe, K.; Lemeur, R. Determining reference values for stem water potential and maximum daily trunk shrinkage in young apple trees based on plant responses to water deficit. *Agric. Water Manag.* **2009**, *96*, 541–550. [[CrossRef](#)]
70. Pantin, F.; Simonneau, T.; Muller, B. Coming of leaf age: Control of growth by hydraulics and metabolics during leaf ontogeny. *New Phytol.* **2012**, *196*, 349–366. [[CrossRef](#)] [[PubMed](#)]
71. Peguero-Pina, J.J.; Sancho-Knapik, D.; Morales, F.; Flexas, J.; Gil-Pelegrín, E. Differential photosynthetic performance and photoprotection mechanisms of three Mediterranean evergreen oaks under severe drought stress. *Funct. Plant Biol.* **2009**, *36*, 453–462. [[CrossRef](#)]
72. Ackerly, D.D.; Bazzaz, F.A. Leaf dynamics, self-shading and carbon gain in seedlings of a tropical pioneer tree. *Oecologia* **1995**, *101*, 289–298. [[CrossRef](#)] [[PubMed](#)]
73. Tinoco-Ojanguren, C.; Pearcy, R.W. A comparison of light quality and quantity effects on the growth and steady-state and dynamic photosynthetic characteristics of three tropical tree species. *Funct. Ecol.* **1995**, *9*, 222–230. [[CrossRef](#)]
74. Fetene, M.; Feleke, Y. Growth and photosynthesis of seedlings of four tree species from a dry tropical afro-montane forest. *J. Trop. Ecol.* **2001**, *17*, 269–283. [[CrossRef](#)]
75. Meir, P.; Levy, P.E.; Grace, J.; Jarvis, P.G. Photosynthetic parameters from two contrasting woody vegetation types in west Africa. *Plant Ecol.* **2007**, *192*, 277–287. [[CrossRef](#)]
76. Riddoch, I.; Grace, J.; Fasehun, F.E.; Riddoch, B.; Ladipo, D.O. Photosynthesis and Successional Status of Seedlings in a Tropical Semi-Deciduous Rain Forest in Nigeria. *J. Ecol.* **1990**, *79*, 491–503. [[CrossRef](#)]
77. Ellis, A.R.; Hubbell, S.P.; Potvin, C. In situ field measurements of photosynthetic rates of tropical tree species: A test of the functional group hypothesis. *Can. J. Bot.* **2000**, *78*, 1336–1347.
78. Domingues, T.F.; Meir, P.; Feldpausch, T.R.; Saiz, G.; Veenendaal, E.M.; Schrodte, F.; Bird, M.; Djagbletey, G.; Hien, F.; Compaore, H.; et al. Co-limitation of photosynthetic capacity by nitrogen and phosphorus in West Africa woodlands. *Plant Cell Environ.* **2010**, *33*, 959–980. [[CrossRef](#)] [[PubMed](#)]
79. Bürkle, L.; Hibberd, J.M.; Quick, W.P.; Kühn, C.; Hirner, B.; Frommer, W.B. The H(+)-sucrose cotransporter NtSUT1 is essential for sugar export from Tobacco leaves. *Plant Physiol.* **1998**, *118*, 59–68. [[CrossRef](#)] [[PubMed](#)]
80. Jahnke, S.; Schlesinger, U.; Feige, G.B.; Knust, E.J. Transport of photoassimilates in young trees of *Fraxinus* and *Sorbus*: Measurement of translocation in vivo. *Bot. Acta* **1998**, *111*, 307–315. [[CrossRef](#)]
81. Wong, J.H.H.; Randall, D.D. Translocation of photoassimilate from leaves of two polyploid genotypes of tall fescue differing in photosynthetic rates. *Physiol. Plant.* **1985**, *63*, 445–450. [[CrossRef](#)]
82. Rennie, E.A.; Turgeon, R. A comprehensive picture of phloem loading strategies. *Proc. Natl. Acad. Sci. USA* **2009**, *106*, 14162–14167. [[CrossRef](#)] [[PubMed](#)]
83. Fu, Q.; Cheng, L.; Guo, Y.; Turgeon, R. Phloem loading strategies and water relations in trees and herbaceous plants. *Plant Physiol.* **2011**, *157*, 1518–1527. [[CrossRef](#)] [[PubMed](#)]
84. Zavaliev, R.; Sagi, G.; Gera, A.; Epel, B.L. The constitutive expression of Arabidopsis plasmodesmal-associated class 1 reversibly glycosylated polypeptide impairs plant development and virus spread. *J. Exp. Bot.* **2010**, *61*, 131–142. [[CrossRef](#)] [[PubMed](#)]
85. Slewinski, T.L.; Braun, D.M. Current perspectives on the regulation of whole-plant carbohydrate partitioning. *Plant Sci.* **2010**, *178*, 341–349. [[CrossRef](#)]
86. Epila, J.; Verbeeck, H.; Otim-Epila, T.; Okullo, P.; Kearsley, E.; Steppe, K. The ecology of *Maesopsis eminii* Engl. in tropical Africa. *J. Afr. Ecol.* **2017**. [[CrossRef](#)]
87. Jensen, K.H.; Savage, J.A.; Holbrook, N.M. Optimal concentration for sugar transport in plants. *J. R. Soc. Interface* **2013**, *10*, 20130055. [[CrossRef](#)] [[PubMed](#)]
88. Scheiter, S.; Langan, L.; Higgins, S.I. Next-generation dynamic global vegetation models: Learning from community ecology. *New Phytol.* **2013**, *198*, 957–969. [[CrossRef](#)] [[PubMed](#)]

